# Supporting Information

Wander et al. 10.1073/pnas.1221127110

## SI Materials and Methods

**Subjects.** This study was completed as a retroactive analysis of previously recorded electrocorticography (ECoG) data. Inclusion criteria for subjects were as follows: (*i*) subjects needed to have participated in the 1D, right justified box task; (*ii*) activity changes in the controlling electrode needed to be driven by overt motor movement or motor imagery; and (*iii*) subjects needed to participate in 50 or more trials. Subjects were not chosen for specific electrode coverage (other than the motor coverage necessary to participate in the task); thus, not all subjects had coverage in all areas discussed. Fig. S2 summarizes the spectrum of coverage for the seven subjects.

It is important to consider the limitations inherent with human ECoG studies. The vast majority of these studies, including the work discussed here, all involve humans with intractable epilepsy. All study subjects were undergoing clinical treatment at the time of their participation in this study. The nature of this subject population should be kept in mind when making extensive cross-subject generalizations and generalizations to healthy populations. Electrode placement was driven by clinical need, and thus not all subjects had coverage of all cortical areas that were discussed above, although in all cases, reported effects were observed in multiple subjects.

**Initial Screening Task.** Before online control, subjects performed overt motor screening to determine candidate electrodes for brain–computer interface (BCI) use. At a visual prompt, subjects were asked to perform gross motor movements of either their tongue or their hand for 3 s. This activity was followed by 3 s of rest. This process was repeated 10–30 times for each of the two motions. They were then asked to repeat this screening process but with imagined movement. Electrodes that demonstrated statistically significant change in high-gamma band (HG) power during activity compared with rest in either or both of these tasks were chosen as candidate controlling electrodes. In cases where there was more than one candidate controlling electrode, the electrode used for online control was chosen based on the magnitude of change between activity and rest and/or neuroanatomical relevance.

**Cortical Reconstructions, Transformations, and Anatomical Labeling.** Preoperative MRI was coregistered with postoperative CT scans using the Statistical Parametric Mapping software package (1). 3D reconstructions of the pial surface were generated using Freesurfer (freely available for download at http://surfer.nmr.mgh.harvard.edu/) and custom code implemented in Matlab (The MathWorks). Electrode positions estimated from postoperative CT were projected to the reconstructed pial surface using the method outlined by Hermes and colleagues (2).

MRI images and projected electrode locations were normalized to Talairach coordinates using Freesurfer. In cases where subjects had electrode coverage of the left hemisphere ($n = 2$), electrode locations were mirrored on to the right hemisphere for cross-comparison with other subjects.

Anatomical labels were estimated using the human motor area template (HMAT) (3) and the Talairach Daemon (4, 5). The HMAT atlas is based on the meta-analysis of 126 motor-based functional MRI (fMRI) studies; thus, it does not include posterior parietal cortex or prefrontal cortex. To account for this, these areas were identified as consisting of Brodmann areas 7/40 and 8/9/46, respectively.

**Estimation of HG Activation Separability and Learning States.** To compare unlearned and learned states, it is necessary to define a trial or trials that delineate these two states. Alternatives exist, such as assuming a continuous learning process or selecting a portion of early trials and late trials to be representative of the learned and unlearned states. However, as performance increases in task, learning typically follow asymptotic trends, and there is no guarantee that users of a task will learn at the same rate, we thought it necessary to use a data-driven approach to determine the transition trial. As performance on the right-justified box (RJB) task saturates quickly, assessment of trends in activation patterns at the controlling electrode itself is a reasonable method for determining this transition trial.

Our algorithm for determining the transition trial makes the following assumptions: (*i*) that there are in fact two states (this does not preclude the existence of more than two states, but our algorithm will only detect a single transition and will effectively group substates), and (*ii*) the the two states can be differentiated by observing changes in a subject's ability to differentially modulate activity at the controlling electrode for up targets compared with down targets.

The transition trial was determined as follows. (*i*) A running estimate of each subject's ability to separate HG activation in up targets compared with down targets was calculated. The mean HG activations for up and down targets were separately smoothed using a Gaussian kernel [five trials full width at half maximum (FWHM)]. Because up and down targets were presented in random sequence, a running difference between smoothed up target and down target activations was calculated by linearly interpolating between observation points. From these operations, an estimate for the difference between activation in up targets and down targets as a function of trial number was established. (*ii*) A model of two distinct Gaussian distributions was fit to the difference estimate such that the difference between these two distributions (measured using the statistic explained below) was maximized. The single free parameter in this model was the transition trial that we are determining.

Distance between the distributions was calculated using the following equation to account not only for differences in the means of the two distributions but also for the variances of the two distributions

$$D_{el} = \frac{\left(\bar{e} - \bar{l}\right)^3}{|\bar{e} - \bar{l}|\sigma_{e:l}^2} \frac{N_e - N_l}{N_{e:l}^2},$$

where $D_{el}$ represents the separability of the early and late trials, $e$ and $l$ represent the early and late trials themselves, respectively, $N_e$ and $N_l$ represent the number of samples in each of these sets, respectively, and $e : l$ represents the joint set of all trials.

When comparing two distributions, this measure represents the proportion of the variance of the joint distribution that can be explained by the difference in the means of the two subdistributions. It has been used previously in the assessment of ECoG signals (6–8).

## SI Results

**Run-by-Run Performance.** As mentioned in the main text, during the task, the cursor traveled from left to right across the screen over the course of 3 s. During this time period, the subject was tasked with causing the cursor to hit the indicated target on the right side of the screen, meaning, that at the end of the 3-s feedback period,

the cursor needed to be within the vertical area defined by that target. In terms of whether or not subjects were able to achieve this requirement, task performance quickly saturated, making assessment of improvement as a function of time impossible. Based on simulated, randomized replay of the task using previously recorded ECoG data that were phase scrambled and random target sequences (144 runs of 17 trials each, totaling 2,448 trials), chance task performance for a given run was 48.8%, with a 95th percentile of 64.7%. Accordingly, if actual performance for a given run exceeded the 95th percentile, then performance on that run can be considered above chance with statistical significance. Fig. S4 shows individual performance trends for each subject on a run-by-run basis. Note that five of the seven subjects were performing above chance by the end of their first run, and performance often saturated quickly, necessitating the use of alternative methods to assess changes in aptitude.

**Behavioral Results Assuming an Optimal Cursor Trajectory.** Additionally, the solution space for how a given subject could achieve success in the RJB is extremely large. Subjects were not asked to report their intended cursor trajectory. If one makes the assumption that the intended cursor trajectory is constant throughout all trials and that the subject asymptotically approaches that trajectory, the intended trajectory can be approximately inferred by looking at the last few trials conducted by each subject. Each individual trial can then be compared with this inferred trajectory, giving an estimate of how well a given subject's performance approached this intended trajectory as they gained experience with the task. In an effort to obtain an understanding of some of the behavioral parameters of the RJB, for the five of seven subjects for whom target trajectories were recorded, we performed this analysis. In three of these five subjects, we saw a statistically significant decrease in mean-squared error (MSE) over the course of all trials performed, compared against an intended trajectory estimated from the last 20% of trials of a given target type. Individual results are shown in Fig. S5.

It is important to note that this method assumes that performance gains are made only by the subject improving their ability to precisely execute an indented trajectory and not by fine tuning of the intended trajectory itself. We find the assumptions made in this analysis were less robust than those used in the primary analysis that uses power changes in the controlling electrode as an assessment of task performance, but they do provide insight into the fact that as subjects gain task experience and exhibit changes in dynamics of neural control, there are concomitant changes in some behavioral aspects of the task.

**Evaluation of Lower-Frequency Cortical Activity.** HG is the range of frequencies that often receives the primary focus of attention in ECoG studies, partially because, until recently (9), it had not been demonstrated that high-frequency signals could be obtained using noninvasive methods. However, the volitional modulation of lower-frequency cortical rhythms such as the mu-beta rhythm (12–30 Hz) is often used as a control signal in noninvasive BCIs (10–13) and is thus worth discussing as a complementary analysis to the HG analysis focused on in the main text of the paper.

Of the 569 electrodes investigated from the seven subjects, we found 128 electrodes showing statistically significant decreases in mu-beta (12–30 Hz) activity between feedback during up targets compared with rest (left-sided two-sample $t$ test, Bonferroni corrected, $27 < N_1 < 98$, $51 < N_2 < 187$; $P < 8.631 \times 10^{-5}$). These findings are shown in Fig. S6. Further, of that same 569 electrodes, we found 123 electrodes showing a statistically significant decrease in mu-beta activity between all targets and rest (left-sided two-sample $t$ test, Bonferroni corrected, $54 < N_1 < 198$, $51 < N_2 < 187$; $P < 6.284 \times 10^{-5}$). Electrodes showing significant activity increase were distributed throughout frontal and parietal cortices. This spatially diffuse, task-related decrease of mu-beta activity is consistent with previous findings that motor-related desynchronization of mu-beta activity is more spatially widespread than increases in HG activity (6). Trial-by-trial patterns showing this activity decrease can be seen in Fig. S6.

Using the same transition trials defined in the main text, we performed a similar analysis to assess whether activation patterns in the mu-beta range changed over the course of transitioning from a learned to an unlearned state. Although there were a few electrodes exhibiting significant changes between these two states, as illustrated in Fig. S6, these changes were less spatially organized and lower in magnitude than HG changes over a similar time period.

**Alternative Methods for Assessment of Learning States.** To assess the robustness of findings with respect to our method for determination of early and late learning states, we performed additional analyses of distributed changes in HG activity comparing the first 30% and the last 30% of all trials recorded for each subject, an approach that has been used previously (14). Other than the definition of the transition period, the method for these analyses was identical to what has been described previously in the main text and *SI Materials and Methods*. As shown in Fig. S7, we found similar spatial patterns showing less HG activation in dorsolateral prefrontal cortex (PFC) and posterior parietal cortex (PPC) in the last 30% of trials compared with the first 30% trials. This result suggests that the observed spatiotemporal patterns in HG activity are robust to alternative methods of segmenting the data in to learning states.


1. Penny W, Friston K, Ashburner J, Kiebel S (2006) *Statistical Parametric Mapping: The Analysis of Functional Brain Images*, ed Nichols T (Academic Press, London), 1st Ed.
2. Hermes D, Miller KJ, Noordmans HJ, Vansteensel MJ, Ramsey NF (2010) Automated electrocorticographic electrode localization on individually rendered brain surfaces. *J Neurosci Methods* 185(2):293–298.
3. Mayka MA, Corcos DM, Leurgans SE, Vaillancourt DE (2006) Three-dimensional locations and boundaries of motor and premotor cortices as defined by functional brain imaging: A meta-analysis. *Neuroimage* 31(4):1453–1474.
4. Lancaster JL, et al. (1997) Automated labeling of the human brain: A preliminary report on the development and evaluation of a forward-transform method. *Hum Brain Mapp* 5(4):238–242.
5. Lancaster JL, et al. (2000) Automated Talairach atlas labels for functional brain mapping. *Hum Brain Mapp* 10(3):120–131.
6. Miller KJ et al. (2007) Spectral changes in cortical surface potentials during motor movement. *J Neurosci* 27(9):2424–2432.
7. Miller KJ, et al. (2010) Cortical activity during motor execution, motor imagery, and imagery-based online feedback. *Proc Natl Acad Sci USA* 107(9):4430–4435.
8. Blakely T, Miller KJ, Zanos SP, Rao RPN, Ojemann JG (2009) Robust, long-term control of an electrocorticographic brain-computer interface with fixed parameters. *Neurosurg Focus* 27(1):E13.
9. Darvas F, et al. (2010) High gamma mapping using EEG. *Neuroimage* 49(1):930–938.
10. McFarland DJ, Lefkowicz AT, Wolpaw JR (1997) Design and operation of an EEG-based brain-computer interface with digital signal processing technology. *Behav Res Methods* 29:337–345.
11. Fabiani GE, McFarland DJ, Wolpaw JR, Pfurtscheller G (2004) Conversion of EEG activity into cursor movement by a brain-computer interface (BCI). *IEEE Trans Neural Syst Rehab Eng* 12(3):331–338.
12. Wolpaw JR, McFarland DJ, Neat GW, Forneris CA (1991) An EEG-based brain-computer interface for cursor control. *Electroencephalogr Clin Neurophysiol* 78(3):252–259.
13. Lemieux L, Allen PJ, Franconi F, Symms MR, Fish DR (1997) Recording of EEG during fMRI experiments: Patient safety. *Magnetic Resonance Med* 38(6):943–952.
14. Koralek AC, Jin X, Long JD, 2nd, Costa RM, Carmena JM (2012) Corticostriatal plasticity is necessary for learning intentional neuroprosthetic skills. *Nature* 483(7389):331–335.

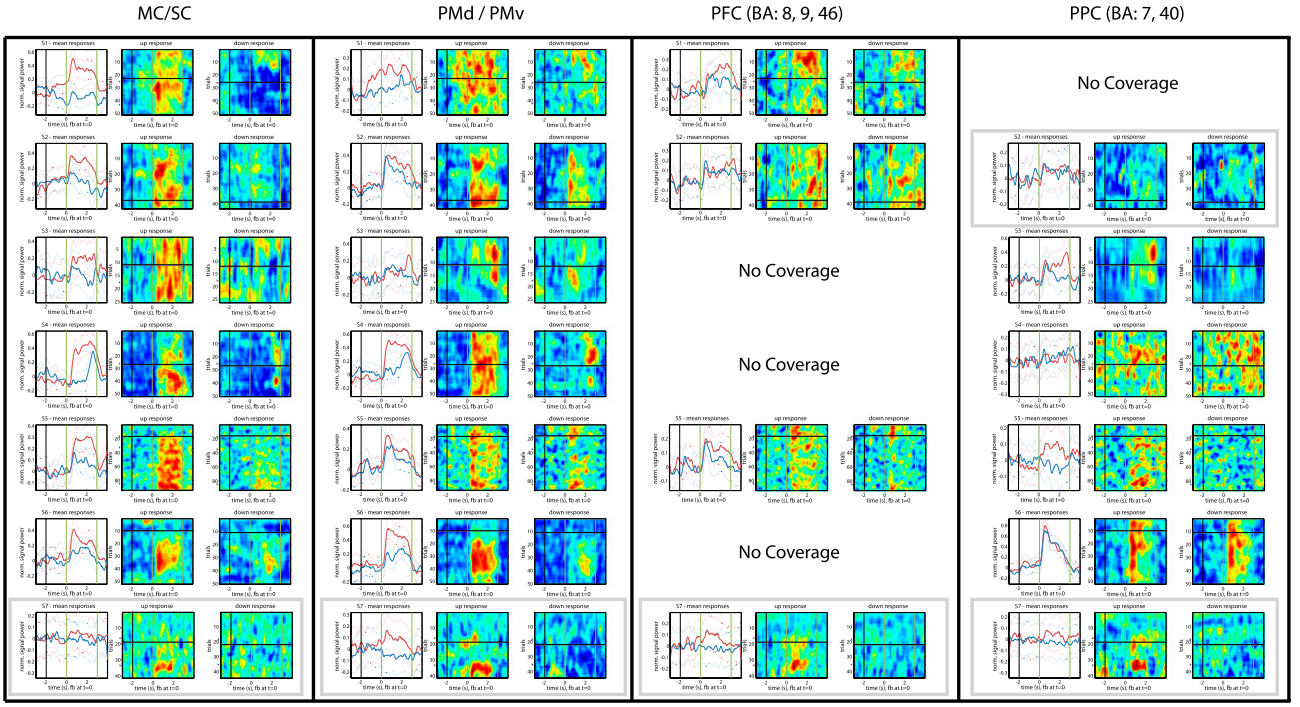


**Fig. S1.** Time by trial high gamma activation for individual subjects. (*Left* subplot) Average high-gamma activation for all trials separated by up and down targets. Phases of the task (ordered from L to R: inter-stimulus interval, target presentation, feedback, reward) are separated by vertical bars. Dotted line represents SEM. Up and down target activations shown in red and blue respectively. (*Center* and *Right* subplots) Trial-by-trial high-gamma activation for all trials, separated by up (*Center* subplot) and down (*Right* subplot) targets. Trial count is shown on the vertical axis, time, as described for the left subplot is shown on the horizontal axis. The black horizontal bar represents the model separation point derived solely from the controlling electrode. Plots surrounded in gray boxes are for electrodes that did not exhibit significant task modulation.

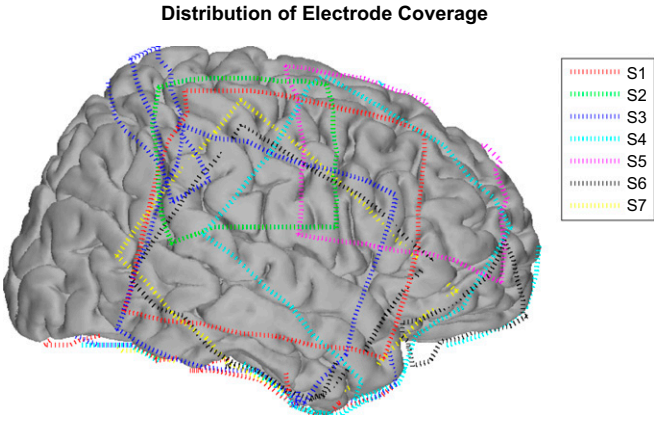


**Fig. S2.** Spatial distribution of electrode coverage. Differences in electrode coverage for the seven study subjects. Dashed lines forming a rectangle or square represent the approximate outlines of grids (8 × 8, 6 × 8, 4 × 8, or 2 × 8). Single dashed lines represent the approximate centerline of strips (1 × 8, 1 × 6, 1 × 4).

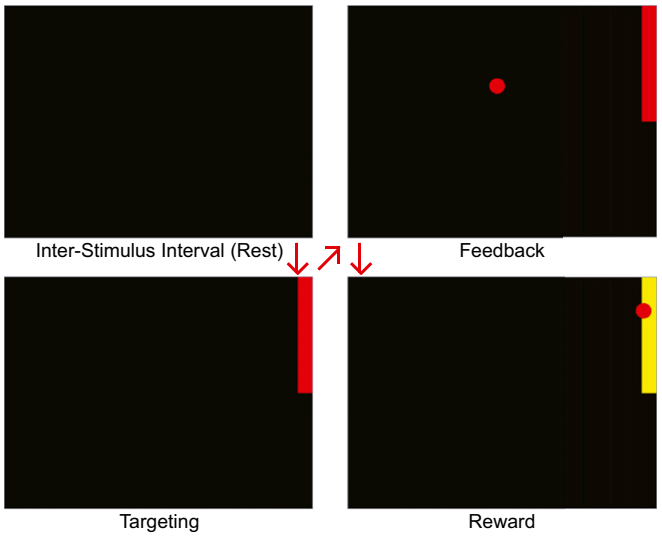


**Fig. S3.** Task overview. Example images of visual feedback presented to subject during binary right-justified box task. Subjects were randomly presented up or down targets during each trial.

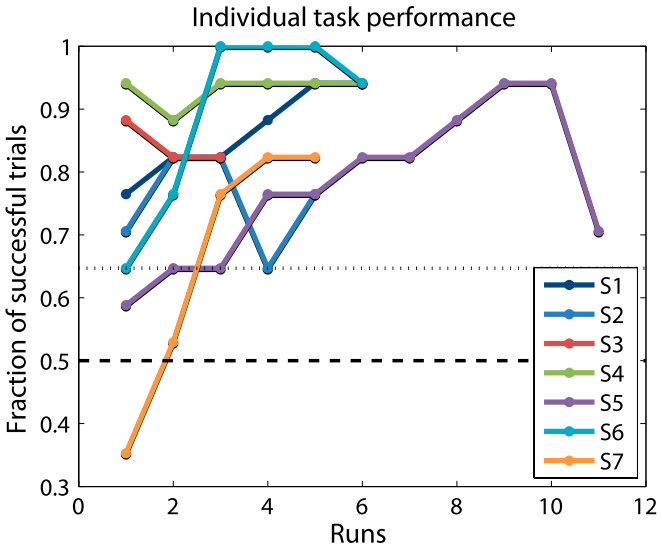


**Fig. S4.** Run-by-run task performance. Task performance for each user shown on a run-by-run basis. The 95th percentile of chance performance is represented in gray. Note that for five of the seven subjects, task performance was above chance by the end of the first run, and for many subjects, performance quickly saturated.

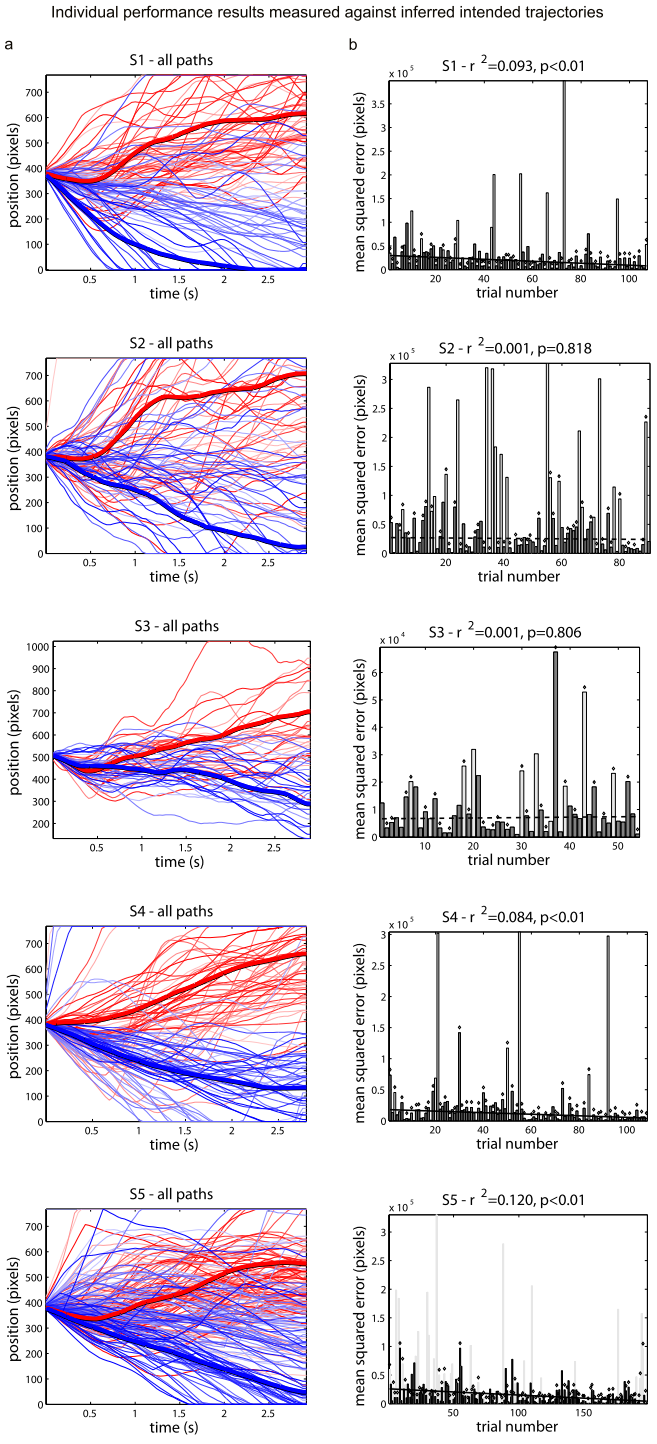


**Fig. S5.** Behavioral analysis of cursor trajectories measured against inferred intended trajectories. (*A*) Recorded trajectories for individual subjects shown as cursor position as a function of time during the feedback phase of the task. Trajectories for up targets are shown in red and for down targets are shown in blue. Earlier and later trials are depicted in lighter and darker shades, respectively. The inferred intended trajectory is shown as a thick red or blue line. (*B*) MSE for each individual trial relative to the inferred intended up and down trajectories. Successful trials shown in dark gray and failed trials are shown in light gray. Up targets are notated with a diamond (◇) above each bar. To assess performance trends we performed logistic regression of MSE values as a function of trial number. Significant trends are shown as solid regression lines; nonsignificant trends are shown as dashed lines.

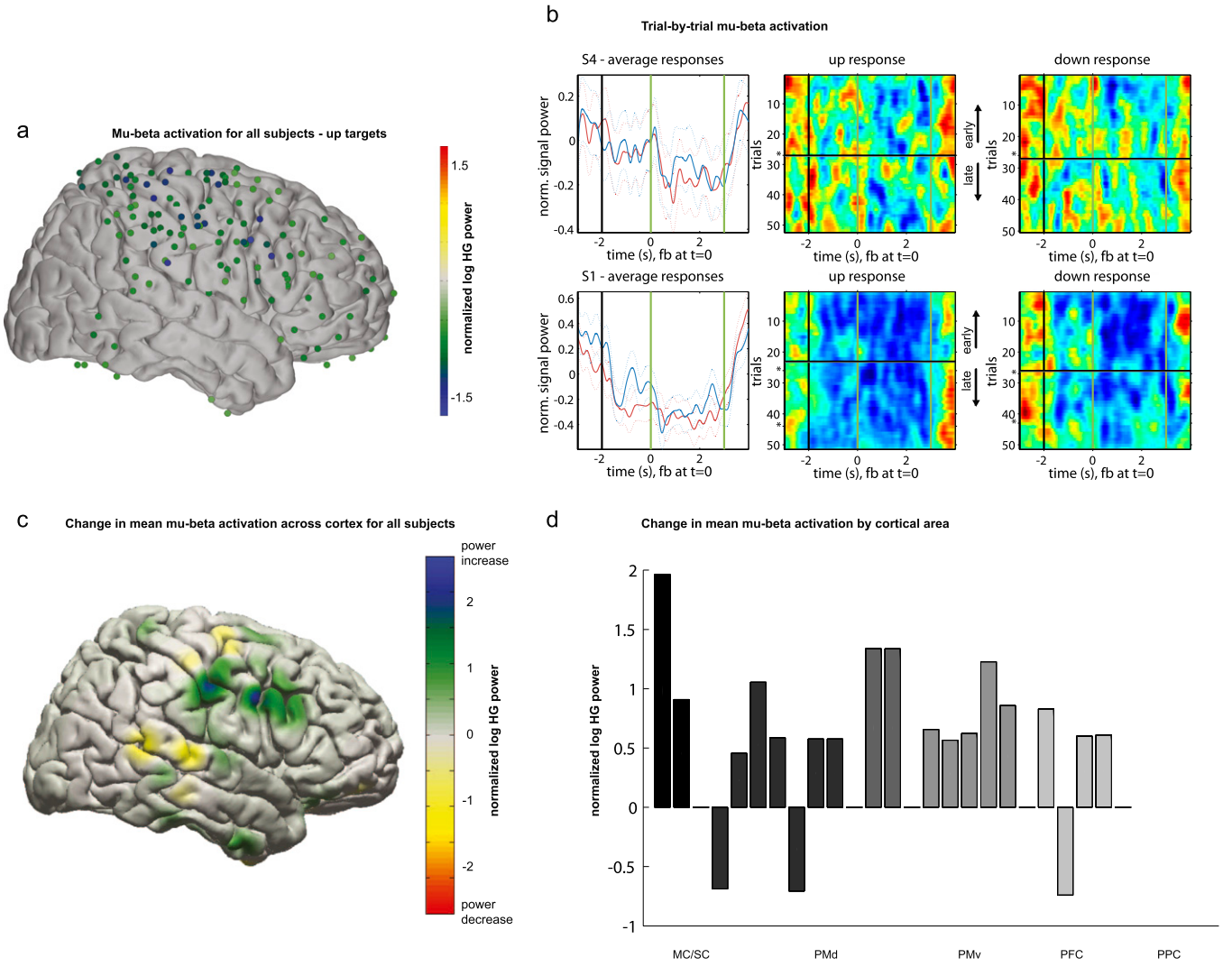


**Fig. S6.** Changes in mu-beta activity patterns. (*A*) Significant decreases (normalized mu-beta power) during up targets for all lateral electrodes for all subjects (left hemispheric coverage projected to right hemisphere) projected on to the Talairach brain. Note widespread cortical activation including frontal, middle-parietal, and posterior-parietal areas. (*B*) Subplot 1: average mu-beta activity patterns in a given electrode from a specific subject for all trials separated by up and down targets. Subject is specified in the subplot title. Phases of the task (ordered from L to R: ISI, target presentation, feedback, reward) are separated by vertical bars. Dotted line represents SEM. Subplots 2 and 3: trial-by-trial mu-beta activity patterns for all trials, separated by up (subplot 2) and down (subplot 3) targets. Trial count is shown on the vertical axis, and breaks in the experimental session of more than 8 h are denoted with an asterisk (*). Time, as described for subplot 1 is shown on the horizontal axis. The black horizontal bar represents the model separation point derived solely from HG activity in the controlling electrode. (*C*) Spatial distribution of change in mean mu-beta activation comparing early to late trials for all targets for all subjects. Activations for individual electrodes are normalized against rest periods from the same electrode for a given run to eliminate gain differences between electrodes and nonstationarities within a given electrode over time. Activation change values are blurred using a 12-cm FWHM Gaussian filter. (*D*) Change in mean mu-beta activation for all electrodes showing significant change from early to late trials, classified in to approximate cortical areas.

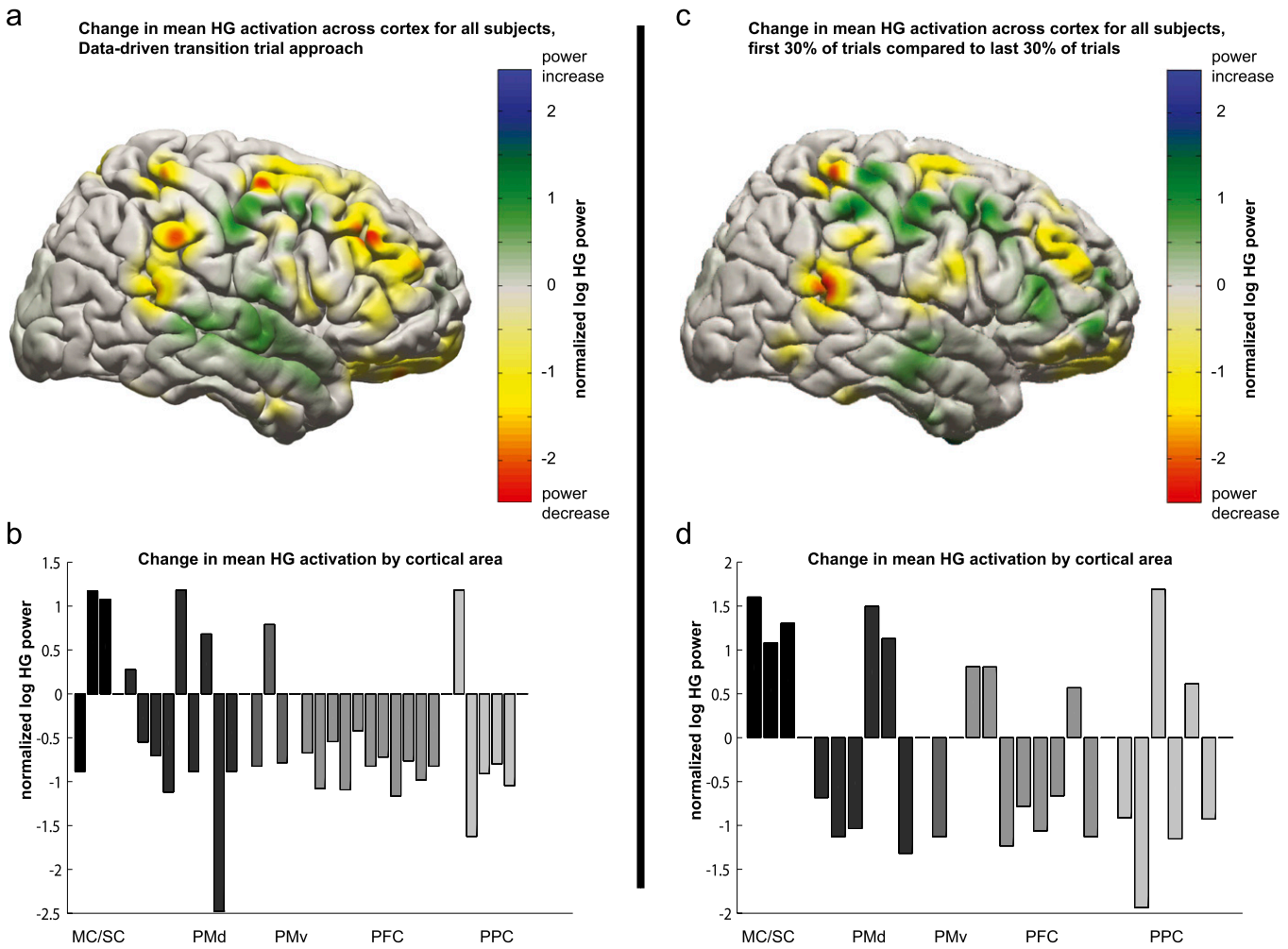


**Fig. S7.** Changes in HG activity patterns observed with alternative data segmentation method. (*A* and *B*) Repetition of Fig. 4, given for direct comparison with the subsequent two panels. (*C*) Spatial distribution of change in mean HG activation comparing the first 30% to the last 30% of all trials recorded for each subject. Note similar spatial patterns compared with *A*. (*D*) Change in HG activation for all electrodes showing significant change from early to late trials, classified in to approximate cortical areas.

**Table S1. Summary of subject population, data collected, and basic statistical analysis**

| ID | Age (y) | Sex | Total runs | Total trials | Up trials | Down trials | Motor movement type | *P* value (up vs. rest) | *P* value (down vs. rest) | Modeled transition trial | Early-late separability ($R^2$) | Early-late *P* value |
|---|---|---|---|---|---|---|---|---|---|---|---|---|
| S1 | 26 | Female | 6 | 108 | 54 | 54 | Overt | <0.0001 | 0.075 | 48 | 0.6422 | <0.0001 |
| S2 | 22 | Male | 5 | 90 | 45 | 45 | Imagined | <0.0001 | 0.994 | 75 | 0.3403 | <0.0001 |
| S3 | 18 | Male | 3 | 54 | 27 | 27 | Overt | <0.0001 | 1 | 22 | 0.8689 | <0.0001 |
| S4 | 27 | Male | 6 | 108 | 54 | 54 | Overt | <0.0001 | 0.983 | 53 | 0.6097 | <0.0001 |
| S5 | 29 | Male | 11 | 198 | 98 | 100 | Imagined | <0.0001 | 0.986 | 32 | 0.4076 | <0.0001 |
| S6 | 32 | Male | 6 | 108 | 54 | 54 | Imagined | <0.0001 | 1 | 20 | 0.2039 | <0.0001 |
| S7 | 25 | Female | 5 | 90 | 45 | 45 | Imagined | 0.271 | 0.0028 | 40 | 0.7695 | <0.0001 |